Relative Timing of Last Glacial Maximum and Late Glacial Events in the central Tropical Andes

Gordon R. M. Bromley[a*], Joerg M. Schaefer[b], Gisela Winckler[b], Brenda L. Hall[a], Claire E. Todd[c], Kurt M. Rademaker[a]

[a]*Department of Earth Sciences and the Climate Change Institute, Edward T. Bryand Global Sciences Center, University of Maine, Orono, ME 04469-5790, USA*

[b]*Lamont-Doherty Earth Observatory, Geochemistry, Route 9W, Palisades, NY 10964, USA*

[c]*Pacific Lutheran University, Tacoma, WA 98447, USA*

*Corresponding author. Tel: +1 207-581-2190; Fax: 207-581-1203;
E-mail: gordon.bromley@umit.maine.edu

ABSTRACT. Whether or not tropical climate fluctuated in synchrony with global events during the Late Pleistocene is a key problem in climate research. However, the timing of past climate changes in the tropics remains controversial, with a number of recent studies reporting that tropical ice-age climate is out of phase with global events. Here, we present geomorphic evidence and an in-situ cosmogenic ^{3}He surface-exposure chronology from Nevado Coropuna, southern Peru, showing that glaciers underwent at least two significant advances during the Late Pleistocene prior to Holocene warming. Comparison of our glacial-geomorphic map at Nevado Coropuna to mid-latitude reconstructions yields a striking similarity between Last Glacial Maximum (LGM) and Late Glacial sequences in tropical and temperate regions.

Exposure ages constraining the maximum and end of the older advance at Nevado Coropuna range between 24.5 and 25.3 ka, and between 16.7 and 21.1 ka, respectively, depending on the cosmogenic production-rate scaling model used. Similarly, the mean age of the younger event ranges from 10 to 13 ka. This implies that (1) the LGM and the onset of deglaciation in southern Peru occurred no earlier than at higher latitudes and (2) that a significant Late Glacial event occurred, most likely prior to the Holocene, coherent with the glacial record from mid and high latitudes. The time elapsed between the end of the LGM and the Late Glacial event at Nevado Coropuna is independent of scaling model and matches the period between the LGM termination and Late Glacial reversal in classic mid-latitude records, suggesting that these events in both tropical and temperate regions were in phase.

Keywords: tropics, Late Pleistocene, glacier, Last Glacial Maximum, cosmogenic dating.

1. Introduction

The role of the tropics in climate change has significant implications both for our understanding of climate change at various timescales and, in turn, for prediction of future climate scenarios. Specifically, the relationships between tropical and extra-tropical climate bear directly on two of the foremost problems in palaeoclimate research: the causes of ice ages and of abrupt climate change. The structure and timing of orbital-scale climate oscillations in the tropics are highly relevant for discriminating among the potential drivers of ice ages, including astronomical forcing, atmospheric water vapour, and CO_2. Moreover, as the energetic powerhouse of the earth, the tropics have huge potential to trigger and/or amplify climate changes (e.g. Pierrehumbert, 1999).

Compelling evidence now exists for major shifts in tropical temperature and precipitation during the Late Pleistocene (ice-core data: Thompson et al., 1995, 1998; lake-core data: Baker et al., 2001a,b; glacial-geologic data: Smith et al., 2005a,b, 2008; Zech et al., 2007, 2008), challenging the traditional view of tropical climatic stability (CLIMAP, 1981). However, estimates of the timing and magnitude of these events remain highly variable, as demonstrated in the comprehensive review of tropical glacial records by Smith et al. (2008). Recent glacial-chronologic research in the Andes of central Peru and northern Bolivia (Smith et al., 2005a,b, 2008) suggested that glaciers there reached their maxima as early as 29-35 ka and were in recession during the global Last Glacial Maximum (LGM; ~17-25 ka), implying that the tropics were out of phase with global climate during the last glacial cycle. Based on a cosmogenic-nuclide glacial chronology from Hawaii, Blard et al. (2007) reported that the climate of the central tropical Pacific remained fully glacial until ~15 ka. This is consistent with the Greenland ice-core temperature record (Andersen et al., 2004) but several millennia after the last glacial termination as expressed in mid-latitude glacier records (~18 ka; Schaefer et al., 2006) and in the Antarctic temperature and CO_2 records (~17-18 ka; Monnin et al., 2001). Correlating their Hawaiian data with the Greenland ice-core record, where significant deglacial warming did not occur until the Bølling-Allerød (14.6 Ka), Blard et al. (2007) concluded that the climate systems of the North Atlantic and central tropical Pacific are linked

atmospherically during glacial periods. Together, these two tropical glacier studies indicate that the LGM and the last termination might not have been regionally or globally synchronous during the Late Pleistocene. In contrast, a high-resolution glacier record from the Eastern Cordillera of Bolivia (Zech et al., 2007, 2008), using ^{10}Be surface-exposure dating, suggests that glaciers in the tropical Andes did follow a pattern similar to glaciers at higher latitude during the Late Pleistocene, substantiating the model of global LGM climate synchrony proposed by Denton et al. (1999) and Schaefer et al. (2006).

To address this important conflict, we are reconstructing Late Pleistocene glacier fluctuations on Nevado Coropuna in southern Peru (Fig. 1a). As sensitive indicators of climate change (Oerlemans, 1994, 2001; Anderson & Mackintosh, 2006), glaciers advance and retreat in response to fluctuations of temperature and precipitation. Through careful reconstruction of former glacier extent and chronologic constraint of moraine records, we can determine both the timing and magnitude of glacier events, and therefore climate change, in glaciated and formerly glaciated regions. The recent development of cosmogenic nuclide surface-exposure dating as a glacial-chronologic tool is resulting in constraint of glacier records in tropical, high-mountain regions (e.g. Farber et al., 2005; Smith et al., 2005a,b, 2008; Zech et al., 2007, 2008) where radiocarbon dating typically is problematic due to a lack of organic material. However, cosmogenic-nuclide production rates in low latitudes/high altitudes remain poorly constrained due to the lack of local production-rate calibration sites. The necessary scaling of the production rates from existing calibration sites at higher latitudes and lower altitudes, including the correction for temporal changes in the geomagnetic field (which are highest in the tropics), remains a considerable source of uncertainty (Balco et al., 2008).

We present new glacial-geomorphic maps of Nevado Coropuna, as well as ^{3}He surface-exposure data from glacial landforms, such as moraines and drift edges. We calculated exposure ages using four currently accepted scaling protocols (Balco et al., 2008) and a global compilation of ^{3}He production-rate calibration data (Goehring et al., in prep.; Table 2, Appendix Tables 2,3,4,5). This approach demonstrates the ambiguity currently

inherent to surface-exposure dating at high elevations in the tropics and, in the absence of local production-rate calibration sites, yields the range of possible glacial chronologies at Nevado Coropuna. We then compare our preliminary ^{3}He chronology from southern Peru to published ^{10}Be chronologies from central Peru (Smith et al., 2005a,b, 2008) and the Cordillera Blanca (Farber et al., 2005). To be internally consistent, we recalculated these datasets using the CRONUS online calculator and production rates given by Balco et al. (2008).

2. Geologic Setting

Nevado Coropuna (6395 m; 15º 33'S, 72º 93'W), located 150 km northwest of the city of Arequipa in the Cordillera Ampato (Fig. 1a), is the largest, highest volcano in Peru and dates back to the Miocene (Venturelli et al., 1978). The mountain is formed primarily of andesite lavas characterised by phenocrysts of pyroxene, plagioclase, titanomagnetite, amphibole and biotite set in a light brown hyalopilitic groundmass (plagioclase and pyroxene microlites: Venturelli et al., 1978). The last period of volcanic activity on Nevado Coropuna produced three prominent andesite flows, shown in Figure 1b. Although the lavas have not been dated, Venturelli et al. (1978) suggested they were formed during the Early Holocene. The surrounding landscape comprises an undulating plateau dissected by deep canyons – including the world's deepest – and topped with high, isolated volcanic peaks. Despite its proximity (~100 km) to the Pacific coast, the prevailing easterly airflow maintains a semi-arid climate at Nevado Coropuna, with most annual precipitation (800-1000 mm: Dornbusch, 1998) arriving during the short summer wet season (December-March). Today, the mountain supports an ice cap of approximately 125 km^2, which is restricted to elevations >5500 m on the north side and >5000 m on the south side. An abundance of large, well-preserved moraines (as much as 100 m high) and other glacial landforms attest to multiple periods when the ice cap was greatly expanded and glaciers existed at far lower elevations than they do at present.

[**Figure 1a/1b]**

3. Methods

3.1 Geomorphology

In the only prior glacial-geomorphic investigation of the Nevado Coropuna region, Dornbusch (2002) identified glacial and periglacial features on the mountain's south-western flank corresponding to a single advance, referred to here as the **C-I** advance. We have expanded this dataset, field-mapping moraines (**C-I** moraines) and drift (**C-I** drift) on all sides of the mountain (Figs. 2 and 3), but focusing on two key areas where the glacial stratigraphy is preserved best: two neighbouring valley systems on the peak's north side – Quebrada (hereafter *Q*.) Ullullo and *Q*. Santiago – and in the region of Lago Pallar Cocha on the western flank (Fig. 1b). In addition, we have identified deposits corresponding to two earlier (pre-**C-I**) glacial episodes and one younger event (**C-II** deposits). We categorised and correlated glacial landforms in the field by position, morphology, and relative weathering characteristics. Also, on the basis of cosmogenic ^{3}He exposure ages, we have assigned an absolute chronology to the record. Here, we focus on the **C-I** and **C-II** deposits.

3.2 Surface-exposure sampling

To constrain the age of the **C-I** deposits, we collected surface-exposure samples from lateral moraines in *Q.* Ullullo and *Q.* Santiago, and from the outer edge of a lobate drift sheet in *Q.* Ullullo (Figs. 2 and 3, Section 4.1). We also collected samples from the **C-I** drift edge in *Q.* Huayllaura on the west side of Nevado Coropuna (Fig. 3). To determine the pattern of deglaciation following the **C-I** maximum, we collected surface-exposure samples from the **C-I** drift sheet along a valley bottom transect in *Q.* Sigue Chico (Fig. 3). These samples were taken from cobbles perched on bedrock outcrops and are not associated with any still-stand or readvance during deglaciation. In *Q.* Santiago, we collected samples from the western **C-II** moraine in order to constrain the termination of this younger readvance (Figs. 2 and 3).

[Figures 2 & 3]

During sampling, we focused on the top surfaces of large (>1 m), stable andesite boulders on the crests of outermost moraines (Fig. 4), and on small boulders and cobbles on thin drift edges. By sampling these outer limits we hoped to constrain the onset of deglaciation from maximum positions. Because the flux of cosmogenic radiation attenuates rapidly with depth (Gosse and Phillips, 2001), we focused on the upper few centimetres (~5 cm) of rock. All samples exhibited signs of glacial erosion, such as moulding, striations, and glacial polish, indicating both that glaciers here were wet-based during the Late Pleistocene and that subsequent erosion of boulder surfaces has been minimal. By selecting only glacially eroded clasts, and assuming that such erosion has effectively removed the former (pre-glaciated) surface (e.g. Briner and Swanson, 1998), we aimed to minimise the likelihood of cosmogenic ^{3}He inheritance from earlier periods of exposure. However, we acknowledge concerns that smaller samples are more prone to shielding by snow and vegetation, resulting in erroneously young ages. The arid climate at Nevado Coropuna, and the short-lived nature of snow observed falling on ice-free surfaces, means it is unlikely that snow cover has had a significant shielding effect on these samples. Shielding by vegetation also is unlikely because of the scarcity of flora on Nevado Coropuna. We also acknowledge the possibility of post-depositional exhumation, especially of smaller samples, due to erosion and/or deflation of glacial deposits. Horizon shielding was measured with a clinometer and calculated using the CRONUS on-line calculator (http://hess.ess.washington.edu/ math/al_be_v22/al_be_multiple_v22.php), yielding negligible corrections (Table 1).

[Figure 4]

3.3 Mineral separation and analysis

We used the concentration of cosmogenic ^{3}He measured in clinopyroxene (augite) separates to calculate the surface-exposure ages from Nevado Coropuna shown in Table 1. Andesite samples first were crushed and sieved to retrieve the 125-250 μm size

fraction. We then used heavy liquids, magnetic separation, and hand-picking to separate the pyroxenes, following the protocol described by (Schäfer et al., 1999).

Gases from the pyroxene separates were released by total extraction at ~1300-1400ºC for fifteen minutes. During extraction the furnace was kept exposed to a liquid nitrogen-cooled charcoal trap for gas purification. Further purification was performed by exposing the gases to a SAES getter at room temperature. Residual gas was collected on a cryogenically cooled trap held at ~13ºK and helium then was separated from neon by heating the trap to 45ºK. Abundance and isotopic analyses were performed with a MAP 215-50 noble gas mass spectrometer calibrated with a known volume of a Yellowstone helium standard (MM) with a $^{3}He/^{4}He$ ratio of $16.45R_{\underline{a}}$, where $R_{\underline{a}} = (^{3}He/^{4}He)_{\underline{air}} = 1.384 \times 10^{-6}$. Mass spectrometry was conducted at Lamont-Doherty Earth Observatory following the protocol of Winckler et al. (2005).

3.4 Exposure age calculations and production rates

We present the ^{3}He ages based on four different, currently accepted scaling procedures given in Balco et al. (2008) for ^{10}Be and ^{26}Al dating, taking into account variations of the geomagnetic field over time. We modified the Balco et al. (2008) protocol for ^{3}He measurements (Goehring et al., in prep.) and based our age calculations on the production-rate value derived from a global compilation of calibration datasets presented by Ackert et al. (2003), Cerling and Craig (1994), Dunai and Wijbrans (2000), Licciardi et al. (1999, 2006), and Blard et al. (2006). We did not use elemental production rates because our compilation of existing production-rate calibration data does not indicate any difference in the ^{3}He production rate between olivine and pyroxene, nor between different olivine studies, despite the difference in elemental composition. To calculate the production rate at the respective sample altitude, we used the scaling factors for spallation only as there is no evidence for muonic production of cosmogenic ^{3}He. We employed a density of 2.7 (Appendix Table 2) and an attenuation length of 165 g/cm^2, and assumed the production rate decreases exponentially with sample thickness (as implemented in the CRONUS Earth web-based calculator, version 2.2). In addition, we calculated the local air pressure at our sites using the European Centre for Medium-range Weather Forecasts

(ECMWF) Re-analysis ERA-40 data (25-year average; Kalberg et al., 2004; Table 1). The derived local air pressure results agree with the values given by the CRONUS Earth online calculator. This approach allows us to (1) evaluate the differences among the local production rate values for the field site based on different scaling procedures (an important contribution to the overall uncertainty of the exposure ages) and (2) to compare the presented ^{3}He ages with previously published ^{3}He and also ^{10}Be surface-exposure ages from other sites in an internally consistent way.

4. Results

Figures 2 and 3 show the new geomorphic maps of the Nevado Coropuna site. We present all sample data, including cosmogenic ^{3}He concentrations, in Table 1 and full helium isotope data in Appendix Table 1. Surface-exposure ages calculated using the Li (Lifton et al., 2005) and Lm (Lal, 1991/Stone, 2000/Nishiizumi et al., 1989) protocols (see Balco et al., 2008) are presented in Table 2 and ages calculated using all four schemes are shown in Appendix Table 2. We focus on the Li and Lm ages because (i) both scaling protocols incorporate tropical geomagnetic variability and (ii) the Lm procedure currently is the most widely used scaling protocol. The disparity between these two datasets (ages differ by as much as 30%; Table 2) reflects the urgency of accurate, local production-rate calibration at low latitude/high altitude sites. In the following, we discuss the Nevado Coropuna data and other tropical data based on the Lm scaling, but stress that all conclusions made below are independent of the choice of scaling procedure.

[Tables 1 & 2]

4.1 C-I deposits

In the north-flowing *Q*. Ullullo and *Q*. Santiago, large lateral **C-I** moraines grading into terminal moraines mark the maximum extent of ice during the Late Pleistocene. Moraine crests are broad and dominated by sandy gravel and small boulders (<1 m high), though

larger boulders (>1 m high) are common. Boulder surfaces exhibit glacially polished and striated surfaces, as well as shallow pitting (≤0.5 cm deep), patchy exfoliation, and moderate staining. The *Q*. Ullullo moraines are the largest on Nevado Coropuna (~100 m of relief) and were deposited by a valley glacier 12 km in length. These moraines descend northward, dropping from ~5100 m to the former terminus at 4600 m (Fig. 2). Approximately midway along the eastern limit in *Q*. Ullullo, a small lobe of drift extends ~250 m beyond the lateral moraine (Fig. 2). Boulders and fines associated with this drift sheet are of the same weathering stage as material on the nearby **C-I** moraines, into which the unit grades. Therefore, we interpret the drift as corresponding to an earlier, slightly more extensive advance during the **C-I** period. Samples NC2, NC3 and NC4 were collected from this limit. A single, low-relief (~2 m) lateral moraine on the east valley side, approximately one kilometre up-valley from the C-**I** terminus, indicates a recessional position (Fig. 2). **C-I** moraines in *Q*. Santiago are as much as 80 high and descend to a terminal elevation of 4730 m (Figs. 1b and 2). Several smaller, discontinuous lateral moraines are located a short distance up-valley from the **C-I** terminal position.

The **C-I** limit on the west flank of Nevado Coropuna comprises both lateral moraines and drift edges (Fig. 3). Surficial boulders and clasts on these landforms exhibit weathering characteristics similar to those of **C-I** deposits on Nevado Coropuna's north side. The moraines occur in valleys formerly occupied by ice tongues and are similar in size, form and weathering stage to those in *Q*. Ullullo and *Q*. Santiago. A key difference is that the former glacier termini on the west flank occurred at lower elevations (as low as 4350 m) than on the north side. On the plateau immediately south of Lago Pallar Cocha, the former limit of ice in *Q*. Huayllaura is marked by a prominent **C-I** drift edge located five kilometres from the current glacier margin. This landform comprises a thin spread of small boulders and cobbles, exhibiting the same weathering characteristics as material on the **C-I** materials, overlying bedrock and slope deposits. In places, such as where samples NC5 and NC8 were collected, the drift sheet extends as much as one kilometre beyond the western lateral moraine (**C-I**) of *Q*. Huayllaura. As with the lobate drift sheet in *Q*.

Ullulo, this indicates that an earlier, more extensive **C-I** advance preceded the deposition of the large **C-I** moraines on the western flank of Nevado Coropuna.

Nine surface-exposure ages from **C-I** limits range from 15.3 ± 0.4 to 25.4 ± 0.8 ka (Table 2; Figs. 2, 3, and 5a), with a mean age of 20.7 ± 3.7 ka (all mean ages reported here are non-error-weighted and given with standard deviation). Sample NC6 (61.3 ± 1.4 ka) is more than 3 σ beyond the mean and therefore was rejected as an outlier. The mean age of samples from the **C-I** drift edge is 20.7 ± 4.7 ka (N=6; Table 2), whereas the mean age of the **C-I** moraines is 21.0 ± 0.2 ka (N=3; Table 2). Steady retreat of ice from the **C-I** limits is demonstrated in *Q*. Sigue Chico by three exposure ages of 19.4 ± 0.4 (4606 m), 16.8 ± 0.4 (4641 m), and 14.9 ± 0.6 ka (4899 m) from drift along a valley-floor transect (Fig. 3). We rejected sample NC14 (35.6 ± 1.0 ka) from the recessional transect on the basis that it is both out of sequence and anomalously old (Table 2).

4.2 C-II deposits

Landforms corresponding to a significant event (**C-II**) postdating the **C-I** maximum are preserved best in *Q*. Ullullo and *Q*. Santiago. **C-II** moraine crests typically are narrow and dominated by small (<1 m high) boulders, cobbles, and gravel. Surficial boulders commonly are striated and glacially polished and exhibit very little staining, pitting, or exfoliation. A closely spaced pair of lateral moraines, as much as 30 m high, occurs on both valley sides in *Q*. Ullullo. These moraines descend to a former terminus at 4700 m, approximately 3.5 km up-valley from the **C-I** terminal position (Fig. 2). In *Q.* Santiago, deposits corresponding to the **C-II** event form a single lateral moraine on the valley's west side that splits near the former terminus (5000 m; 3.5 km up-valley from the **C-I** terminus) into two closely spaced ridges (Fig. 2). In places where the western lateral moraine crosses small (1-4 m high) bedrock scarps, it loses its ridge form and is represented by a line of glacially moulded and striated boulders and cobbles perched on bedrock. Farther east, a section of **C-II** moraine occurs high on the west side of Queña Ranra (hereafter *Q*. Ranra; Fig. 1b), dropping from 5250 m to 5120 m, whereupon the landform disappears beneath an andesite flow (Fig. 2). At ~5200 m the descending lateral moraine splits to form two parallel ridges that are similar in relief, morphology, and

boulder weathering to those in *Q*. Santiago and *Q*. Ullullo. On the west side of Coropuna, a short (~500 m) segment of **C-II** moraine protrudes from beneath the andesite flow in upper *Q*. Sigue Chico (Fig. 3). The landform is similar in size, position, morphology, and weathering to **C-II** deposits on Coropuna's north side. Thus far, we have been unable to map **C-II** deposits on the mountain's south side. In *Q*. Santiago, the prominent **C-II** moraine is constrained by four ages ranging from 10.6 ± 0.3 to 14.2 ± 0.3 ka, with a mean age of 13.0 ± 1.6 ka (Table 2; Figs. 2, 3 and 5a).

4.3 Pre-C-I deposits

Figures 2 and 3 show the distribution of deposits corresponding to two earlier (pre-**C-I**) glaciations at Nevado Coropuna. The most extensive deposits (shown as green in Figures 2 and 3) occur on all but the west side of the mountain as distinct but broad-crested lateral moraines and weathered drift. Boulders associated with these deposits are visibly more weathered than **C-I** boulders, exhibiting deep (>1 cm) pits, moderate-to-widespread surface exfoliation, and extensive staining. In *Q*. Huayllaura, lateral moraines as much as 80 m high extend three kilometres down-valley from the **C-I** terminus (Fig. 3) to an elevation of 4150 m. On the mountain's north side, older lateral moraines in *Q*. Ullullo and *Q*. Santiago, between 2 and 10 m in relief, occur immediately distal to the large **C-I** lateral moraines (Fig. 2). Extensive pre-**C-I** drift occurs on the plateau north and east of *Q*. Ranra and in the undulating hills west of *Q*. Ullullo (Fig. 3). A remnant of an even older drift sheet (shown as brown in Figs. 2 and 3) is preserved on a hilltop east of the **C-I** terminus in *Q*. Santiago. The drift comprises boulders that are heavily stained and severely exfoliated, and that exhibit minor cavernous weathering. We did not observe any pre-**C-I** deposits on the west side of Nevado Coropuna.

5. Discussion

Our ^{3}He data suggest that glaciers on Nevado Coropuna occupied their maximum Pleistocene extent between ~15 and 25 ka BP, consistent with the classic LGM during Marine Isotope Stage 2. The mean age of the LGM drift edge (20.7 ± 4.7 ka) is slightly younger than that of the LGM moraines (20.9 ± 0.2 ka**)**, but the stratigraphic relationship of the deposits precludes the drift edge from being younger than the moraines (see Section 4). We suspect that the relatively large spread of exposure ages from the drift edge represents post-depositional exhumation of some of the cobble samples, resulting in the tri-modal age distribution shown in Figure 5. This process would bias the drift edge's mean age to be younger than the true age of deposition. The three older samples (NC4, NC5, NC7: mean age = 24.9 ± 0.5 ka) show high internal consistency. Taken together, we speculate that the best age for the LGM drift edge might be 24.9 ± 0.5 ka ('oldest age mode' in Fig. 5A), and thus several thousand years older than the moraines. We interpret the **C-I** moraine ages as representative of the end of the LGM at Nevado Coropuna. Post-LGM recession over a period of ~6-7 ka was followed by the **C-II** event, dated to 13.0 ± 1.6 ka (mean age), during the Late Glacial period. Given the prominent nature of the lateral moraines, and their continuation as terminal moraines, we suggest that the **C-II** landforms represent a strong readvance as opposed to a period of glacier stillstand during recession. Subsequently, Nevado Coropuna's glaciers retreated to their Late Holocene and modern configuration.

Though the exposure ages given here may shift upon local calibration of cosmogenic-nuclide production, the relative timing of events at Nevado Coropuna will remain the same. Consequently, we are able to make a number of robust and important chronologic conclusions that are independent of the production-rate scaling problem. First, our results show that the maximum extent of glaciers at Nevado Coropuna occurred during Marine Isotope Stage 2 and therefore was broadly synchronous with global events using any of the four scaling schemes. This is consistent with the ^{10}Be glacial chronology from the Cordillera Real, Bolivia (Fig. 1a), presented by Zech et al. (2007, 2008) that shows glaciers were at their maxima during the global LGM. Second, the Late Glacial

readvance of Nevado Coropuna's glaciers during deglaciation was broadly coincident with similar events elsewhere in the tropical Andes (Mercer and Palacios, 1977; Farber et al., 2005; Smith et al., 2008, and references therein; Zech et al., 2007, 2008) and in Hawaii (Pigati et al., 2008), and with advances at higher latitudes in both hemispheres during the Late Glacial period (e.g. Ackert et al., 2008; Briner et al., 2002; Fogwill and Kubik, 2005; Glasser et al., 2006; Ivy-Ochs et al., 1999, 2006, 2008; Kaplan et al., 2008, and references therein; Licciardi et al., 2004; Rinterknecht et al., 2004; Schaefer et al., 2006). Third, the period of time between the abandonment of the LGM moraines and the Late Glacial readvance was ~6-7 ka. This is comparable to the period of time between the LGM termination and Late Glacial events in New Zealand (Ivy-Ochs et al., 1999, 2006, 2009; Schaefer et al., 2006), North America (Gosse et al., 1995a,b; Licciardi et al., 2004; Licciardi et al., 2008), and Switzerland (Ivy-Ochs et al., 1999, 2004), suggesting a coherent pattern of LGM and Late Glacial glaciations in the tropics and higher latitudes of both hemispheres.

Comparison of our record to the detailed ^{10}Be chronology for central Peru/northern Bolivia (Smith et al., 2005a,b, 2008) reveals an apparent conflict regarding the timing of the LGM in the tropics. The extensive dataset presented by Smith et al. (2005a), based on surface-exposure ages from moraines adjacent to the Junin Plain and in the Cordillera Real (Fig. 1a), suggests that the LGM in the Andes (termed the 'local last glacial maximum' or LLGM) occurred as early as 34 ka and, therefore, was out of phase with higher latitudes. Smith et al. (2005b) later revised the dataset using an improved geomagnetic correction, resulting in slightly younger age ranges for the moraines. More recent recalculation of these data using the CRONUS online calculator (version 2.2) and Lm scaling (Balco et al., 2008) resulted in yet younger age ranges for the moraines, but did not alter the authors' conclusion that the LLGM in the Junin region occurred before the global LGM (Smith et al., 2008). These findings are in close agreement with lake-core data from Lakes Titicaca and Junin (Seltzer et al., 2002), Peru. An early LLGM and corresponding period of deglaciation would have major implications for our understanding of the mechanisms driving tropical and global climate change.

Appendix table 3 shows the Junin, central Peru, ^{10}Be dataset of Smith et al. (2005a) recalculated using the CRONUS online calculator and the same set of scaling schemes as outlined in Section 3.4 (see Smith et al. (2008) supporting information Table 5 for entire recalculated dataset). When calculated in this internally consistent way and displayed as age-probability curves (Fig. 5, panel B), the ^{10}Be chronology from central Peru shows broad agreement with the Nevado Coropuna ^{3}He chronology (Fig. 5, panel A). The recalculated 'early LLGM' ages (Group C in Smith et al., 2005a,b) almost uniformly show a distribution comparable to higher-latitude Late Pleistocene glacier maxima (Marine Isotope Stage 2; e.g. Barrows et al., 2002; Ivy-Ochs et al., 2004, 2006, 2009; Kaplan et al., 2004; Licciardi et al., 2008), giving a mean moraine age of 26.7 ± 3.0 ka. Recalculation of the Junin Group B dataset yields a mean age of 16.1 ± 1.7 ka for the moraines. Group B moraines are described by Smith et al. (2005a) as representing a post-LLGM readvance or stillstand, and the recalculated ages are in agreement with that interpretation.

[Figure 5]

Figure 5 (panel C) also depicts the ^{10}Be chronology of Farber et al. (2005) from Quebradas Cojup and Llaca in the Cordillera Blanca, recalculated using the CRONUS online calculator and the same set of scaling schemes as outlined in Section 3.4. Recalculation made the dataset only slightly (<5%) younger than originally published (see Appendix Table 4). As described in detail by Farber et al. (2005), the ages correspond to two groups of moraines – the Rurec moraines and Laguna Baja moraines (after Rodbell, 1993) – interpreted as representing the LLGM and a deglacial stillstand/readvance, respectively. Despite the age distribution (Fig. 9, Farber et al., 2005; Fig. 5, panel C, this study), the authors suggested that the oldest ages in the Rurec dataset correspond to the true age of the moraines, leading them to conclude that glaciers in the western Cordillera Blanca had attained their maximum positions by ~29 ka (Farber et al., 2005). In addition, Farber et al. (2005) correlated the younger Laguna Baja moraines, located ~3 km farther up-valley, with the Group B limits of Smith et al. (2005ab), noting similarities in position and age between the two deposits. On this basis, Farber et al.

(2005) suggested that a high degree of coherence exists between their chronology and that of Smith et al. (2005a,b). Based on the age distribution shown in Figure 5 (panel C), we postulate that the Rurec moraines (mean age 20.0 ± 2.0 ka) were deposited closer to 20 ka than to 30 ka, contemporary with the **C-I** advance at Nevado Coropuna. Furthermore, given both the stratigraphic position of the Laguna Baja moraines and the mean age of the group (14.7 ± 0.9 ka), we tentatively suggest that these deposits correspond broadly to the late-glacial **C-II** moraines on Nevado Coropuna (Fig. 5). We stress, however, that the age distribution of the Laguna Baja samples precludes detailed comparison of the two datasets.

If calculated consistently, the **C-I** (Nevado Coropuna), Group C (Junin), and Rurec (Cordillera Blanca) chronologies are similar, indicating that the glacial events were broadly concurrent. The recalculated data from Hawaii (Appendix Table 5) show that glaciers in the central Pacific also were at their maximum Pleistocene extent during the global LGM. By this scenario, based on the striking similarities in glacial stratigraphy (Fig. 2), the agreement of the Nevado Coropuna chronology with higher-latitude records, and the uniform ~6000-7000 year interval between the LGM termination and the end of the Late Glacial event, we suggest that glacial events in the tropical Andes, and in Hawaii, were broadly in phase with glaciations in the mid-latitudes of both hemispheres during the Late Pleistocene. This conclusion supports a growing body of evidence for synchrony of tropical and higher-latitude climate change (e.g. Mercer and Palacios, 1977; Clapperton, 2000; Baker et al., 2001b; Fritz et al., 2004; Zech et al., 2007, 2008).

6. Conclusions

Our glacial-geomorphic mapping and preliminary ^{3}He data indicate that glaciers on Nevado Coropuna advanced and retreated broadly in phase with higher latitude glaciers during the LGM and Late Glacial period, suggesting that the climate of southern Peru is closely integrated with that of the mid- and high-latitudes in both hemispheres. Taking into account uncertainties in tropical cosmogenic-nuclide production rates, our data

indicate that it is unlikely that the LGM at this site occurred any earlier than at higher latitudes. Moreover, the period of ~6.5 ka between the end of the LGM and the Late Glacial readvance at Nevado Coropuna, a value independent of production-rate scaling, matches the same interval reported in classic records from higher latitudes.

The apparent discrepancy between our data and the extensive ^{10}Be glacier records published from Peru (Farber et al., 2005; Smith et al., 2005a,b, 2008) prompted us to compare the datasets in an internally consistent manner. Based on this approach, we find no evidence of significant temporal discrepancy between our record and recalculated ^{10}Be data, indicating that Late Pleistocene glaciation was broadly synchronous in the central and southern Peruvian Andes and, consequently, in phase with higher-latitude events. Similarly, consistently calculated ^{3}He ages for the LGM termination on Hawaii (Blard et al., 2007) agree with our LGM data, suggesting that the general pattern of Late Pleistocene glaciation was similar throughout the tropics.

Acknowledgements

We thank Ermitaño Zúñiga of Mauca Llacta, Peru, for his invaluable local knowledge and his logistical support during fieldwork. We also acknowledge Marty Yates for conducting elemental measurements, Brent Goehring for compiling, modelling, and calculating production-rate data, and Aaron Putnam for helpful insight and assistance with figures. Funding for the fieldwork was generously provided by the Churchill Foundation, the Geological Society of America Graduate Student Research Grant programme, and the Sigma Xi Grants-in-aid-of-research programme. JMS acknowledges the support of the Comer Science and Educational Foundation. GW thanks Linda Baker for help with the helium analyses and Martin Stute for continuing support of the LDEO noble gas laboratory. We are grateful to two reviewers who made suggestions that greatly improved this manuscript. This is LDEO contribution #XXXX.

References

Ackert, R.P., Singer, B.S., Guillo, H., Kaplan, M.R., Kurz, M.D., 2003. Long-term cosmogenic He-3 production rates from Ar-40/Ar-39 and K-Ar dated Patagonian lava flows at 47 degrees S. Earth and Planetary Science Letters 210, 119-136.

Ackert, R.P.Jr., Becker, R.A., Singer, B.S., Kurz, M.D., Caffee, M.W., Mickelson, D.W., 2008. Patagonian glacier response during the Late Glacial-Holocene transition. Science 321, 392-395.

Andersen, K., Azuma, N., Barnola, J.-M., Bigler, M., Biscaye, P., Caillon, N., Chappellaz, J., Clausen, H., Dahl-Jensen, D., Fischer, H., Flückiger, J., Fritzsche, D., Fujii, Y., Goto-Azuma, K., Grønvold, K., Gundestrup, N., Hansson, M., Huber, C., Hvidberg, C., Johnsen, S. J., Jonsell, U., Jouzel, J., Kipfstuhl, S., Landais, A., Leuenberger, M., Lorrain, R., Masson-Delmotte, V., Miller, H., Motoyama, H., Narita, H., Popp, T., Rasmussen, S., Raynaud, D., Rothlisberger, R.; Ruth, U., Samyn, D., Schwander, J., Shoji, H., Siggard-Andersen, M.-L., Steffensen, J., Stocker, T., Sveinbjörnsdóttir, A., Svensson, A., Takata, M., Tison, J.-L., Thorsteinsson, Th., Watanabe, O., Wilhelms, F., White, J., 2004. High-resolution record of Northern Hemisphere climate extending into the last interglacial period. Nature 431, 147-151.

Anderson, B. and Mackintosh, A., 2006. Temperature change is the major driver of late-glacial and Holocene glacier fluctuations in New Zealand. Geology 34, 121-124.

Baker, P.A., Rigsby, C.A., Seltzer, G.O., Fritz, S.C., Lowenstein, T.K., Bacher, N.P. and Vellz, C., 2001a. Tropical climate changes at millennial and orbital timescales on the Bolivian altiplano. Nature 409, 698-701.

Baker, P.A., Seltzer, G.O., Fritz, S.C., Dunbar, R.B., Grove, M.J., Tapia, P.M., Cross, S.L., Rowe, H.D. and Broda, J.P., 2001b. The history of South American tropical precipitation for the past 25,000 years. Science 291, 640-643.

Balco, G, Stone, J.O., Lifton, N.A. and Dunai, T.J., 2008. A complete and easily accessible means of calculating surface exposure ages or erosion rates from Be-10 and Al-26 measurements. Quaternary Geochronology 3, 174-195.

Barrows, T.T., Stone, J.O., Fifield, L.K. and Cresswell, R.G., 2002. The timing of the Last Glacial Maximum in Australia. Quaternary Science Reviews 21, 159-173.

Blard, P.H., Pik, R., Lave, J., Bourles, D., Burnard, P.G., Yokochi, R., Marty, B. and Trusdell, F., 2006. Cosmogenic He-3 production rates revisited from evidence of grain-size dependent release of matrix-sited helium. Earth and Planetary Science Letters 247, 222-234.

Blard, P.H., Lave, J., Pik, R., Wagnon, P. and Bourles, D., 2007. Persistence of full glacial conditions in the central Pacific until 15,000 years ago. Nature 449, 591-594.

Briner, J.P. and Swanson, T.W., 1998. Using inherited cosmogenic ^{36}Cl to constrain glacial erosion rates of the Cordilleran Ice Sheet. Geology 26, 3-6.

Briner, J.P., Kaufman, D.S., Werner, A., Caffee, M., Levy, L., Manley, W.F., Kaplan, M.R. and Finkel, R.C., 2002. Glacier readvance during the late glacial (Younger Dryas?) in the Ahklun Mountains, southwestern Alaska. Geology 30, 679-682.

Carcaillet, J.T., Bourles, D.L. and Thouveny, N., 2004. Geomagnetic dipole moment and ^{10}Be production rate intercalibration from authigenic $^{10}Be/^{10}Be$ for the last 1.3 Ma. Geochemistry Geophysics Geosystems 5, doi:10.1029/2003GC000641.

Cerling, T.E. and Craig, H., 1994. Cosmogenic ^{3}He production rates from 39ºN to 46ºN latitude, western USA and France. Geochimica et Cosmochimica Acta 58, 249-255.

Clapperton, C., 2000. Interhemispheric synchroneity of Marine Oxygen Isotope Stage 2 glacier fluctuations along the American cordilleras transect. Journal of Quaternary Science 15, 435-468.

Clark, D.H. and Gillespie, A.R., 1997. Timing and significance of late-glacial and Holocene cirque glaciation in the Sierra Nevada, California. Quaternary International 38-9, 21-38.

CLIMAP, 1981. Seasonal reconstructions of the Earth's surface at the last glacial maximum. Geological Society of America Map and Chart Series MC-36, Geological Society of America.

Denton, G.H., Heusser, C.J., Lowell, T.V., Moreno, P.I., Andersen, B.G., Heusser, L.E., Schlüchter, C. and Marchant, D.R., 1999. Interhemispheric linkage of paleoclimate during the last glaciation: Geografiska Annaler 81(A), 107–153.

Dornbusch, U., 1998. Current large-scale climatic conditions in southern Peru and their influence on snowline altitudes. Erdkunde 52, 41-54.

Dornbusch, U., 2002. Pleistocene and present day snowline rise in the Cordillera Ampato. Neues Jahrbuch für Geologie und Paläontologie Abhandlungen 225, 103-126.

Dunai, T.J., 2000. Scaling factors for production rates of in situ produced cosmogenic nuclides: a critical re-evaluation. Earth and Planetary Science Letters 176, 157-169.

Dunai, T.J., 2001. Influence of secular variation of the geomagnetic field on production rates of in situ produced cosmogenic nuclides. Earth and Planetary Science Letters 193, 197-212.

Dunai, T.J. and Wijbrans, J.R., 2000. Long-term cosmogenic ^{3}He production rates (158 ka – 1.3 Ma) from ^{40}Ar/^{39}Ar dated basalt flows at 29ºN latitude. Earth and Planetary Science Letters 176, 147-156.

Farber, D.L., Hancock, G.S., Finkel, R.C. and Rodbell, D.T., 2005. The age and extent of tropical alpine glaciation in the Cordillera Blanca, Peru. Journal of Quaternary Science 20, 759-776.

Fogwill, C.J. and Kubik, P.W., 2005. A glacial stage spanning the Antarctic Cold Reversal in Torres del Paine (51ºS), Chile, based on preliminary cosmogenic exposure ages. Geografiska Annaler (Series A) 87, 403-408.

Fritz, S.C., Baker, P.A., Lowenstein, T.K., Seltzer, G.O., Rigsby, C.A., Dwyer, G.S., Tapia, P.M., Arnold, K.K., Ku T.-L. and Luo, S., 2004. Hydrologic variation during the last 170,000 years in the southern hemisphere tropics of South America. Quaternary Research 61, 95-104.

Glasser, N.F., Harrison, S., Ivy-Ochs, S., Duller, G.A.T. and Kubik, P.W., 2006. Evidence from the Rio Bayo valley on the extent of the North Patagonian Icefield during the Late Pleistocene-Holocene transition. Quaternary Research 65, 70-77.

Gosse, J.C., Klein, J., Evenson, E.B., Lawn, B. and Middleton, R., 1995a. Beryllium-10 dating of the duration and retreat of the Last Pinedale Glacial Sequence. Science 268, 1329-1333.

Gosse, J.C., Evenson, E.B., Klein, J., Lawn, B. and Middleton, R., 1995b. Precise cosmogenic 10Be measurements in western North America: support for a global YD cooling event. Geology 23, 877-880.

Gosse, J.C. and Phillips, F.M., 2001. Terrestrial in situ cosmogenic nuclides: Theory and application. Quaternary Science Reviews 20, 1475–1560.

Guyodo, Y. and Valet, J.-P., 1999. Global changes in intensity of the Earth's magnetic field during the past 800 kyr. Nature 399, 249-252.

Ivy-Ochs, S., Schlüchter, C., Kubik, P. and Denton, G.H., 1999. Moraine exposure ages imply synchronous Younger Dryas glacier advances in the European Alps and in the Southern Alps of New Zealand. Geografiska Annaler 81(A), 313-323.

Ivy-Ochs, S., Schaefer, J., Kubik, P.W., Synal, H-A. and Schlüchter, C, 2004. Timing of deglaciation on the northern Alpine foreland (Switzerland). Eclogae Geologicae Helvetiae 97, 47-55.

Ivy-Ochs, S., Kerschner, H., Reuther, A., Maisch, M., Sailer, R., Schaefer, J., Kubik., P., Synal, H.-A. and Schlüchter, C., 2006. The timing of glacier advances in the northern European Alps based on surface exposure dating with cosmogenic ^{10}Be, ^{26}Al, ^{36}Cl, and ^{21}Ne. Geological Society of America Special Paper 415, 43-60.

Ivy-Ochs, S., Kerschner, H., Reuther, A., Preusser, F., Heine, K., Maisch, M., Kubik., P. and Schlüchter, C., 2008. Chronology of the last glacial cycle in the European Alps. Journal of Quaternary Science 23, 559-573.

Kalberg, P., Simmons, A., Uppala, S. and Fuentes, M., 2004. The ERA-40 archive. ERA-40 Project report series no 17, ECMWF.

Kaplan, M.R., Ackert, R.P., Singer, B.S., Douglass, D.C. and Kurz, M.D., 2004. Cosmogenic nuclide chronology of millennial-scale glacial advances during O-isotope stage 2 in Patagonia. GSA Bulletin 116, 308-321.

Kaplan, M.R., Moreno, P.I. and Rojas, M., 2008. Glacial dynamics in southernmost South America during Marine Isotope Stage 5e to the Younger Dryas chron: a brief

review with a focus on cosmogenic nuclide measurements. Journal of Quaternary Science 23, 649-658.

Lal, D., 1991. Cosmic ray labelling of erosion surfaces: *in situ* nuclide production rates and erosion models. Earth and Planetary Science Letters 104 424-439.

Licciardi, J.M., Kurz, M.D., Clark, P.U. and Brook, E.J., 1999. Calibration of cosmogenic ^{3}He production rates from Holocene lava flows in Oregon, USA, and effects of Earth's magnetic field. Earth and Planetary Science Letters 17, 261-271.

Licciardi, J.M., Clark, P.U., Brook, E.J., Elmore, D. and Sharma, P., 2004. Variable response of western U.S. glaciers during the last deglaciation. Geology 32, 81-84.

Licciardi, J.M., Kurz, M.D. and Curtice, J.M., 2006. Cosmogenic He-3 production rates from Holocene lava flows in Iceland. Earth and Planetary Science Letters 246, 251-264.

Licciardi, J.M. and Pierce, K.L., 2008. Cosmogenic exposure-age chronologies of Pinedale and Bull Lake glaciations in greater Yellowstone and the Teton Range, USA. Quaternary Science Reviews 27, 814-831.

Lifton, N.A., Bieber, J.W., Clem, J.M., Duldig, M.L., Evenson, P., Humble, J.E. and Pyle, R., 2005. Addressing solar modulation and long-term uncertainties in scaling secondary cosmic rays for in situ cosmogenic nuclide applications. Earth and Planetary Science Letters 239, 140-161.

Mercer, J.H. and Palacios, O.P., 1977. Radiocarbon dating the last glaciation in Peru. Geology 5, 600-604.

Monnin, E, Indermühle, A., Dällenbach, D., Flückiger, J., Stauffer, B., Stocker, T.F., Raynaud, D. and Barnola, J.-M., 2001. Atmospheric CO_2 Concentrations over the Last Glacial Termination. Science 291, 112-114.

Nishiizumi, K., Winterer, E.L., Kohl, C.P., Klein, J., Middleton, R., Lal, D. and Arnold, L.D., 1989. Cosmic-ray production-rates of Be-10 and Al-26 in quartz from glacially polished rocks. Journal of Geophysical Research-Solid Earth and Planets 94, 17907-17915.

Oerlemans, J., 1994. Quantifying global warming from the retreat of glaciers. Science 264, 243-245.

Oerlemans, J., 2001. Glaciers and Climate Change. A.A. Balkema Publishers, Rotterdam.

Ohno, M. and Hamano, Y., 1992. Geomagnetic poles over the past 10,000 years. Geophysical Research Letters 19, 1715-1718.

Pierrehumbert, R.T., 1999. Subtropical water vapour as a mediator of rapid climate change. Geophysical Monograph 112, 339-361.

Pigati, J.S., Zreda, M., Zweck, C., Almasi, P.F., Elmore, D. and Sharp, W.C., 2008. Ages and inferred causes of Late Pleistocene glaciations on Mauna Kea, Hawai'i. Journal of Quaternary Science 23, 683-702.

Rinterknecht, V.R., Clark, P.U., Raisbeck, G.M., Yiou, F., Brook, E.J., Tschudi, S. and Lunkka, J.P., 2004. Cosmogenic ^{10}Be dating of the Saupalsselkä I moraine in southwestern Finland. Quaternary Science Reviews 23, 2283-2289.

Rodbell, D.T., 1993. Subdivisions of late Pleistocene moraines in the Cordillera Blanca, Peru, based on rock-weathering features, soils, and radiocarbon dates. Quaternary Research 39, 133-142.

Schäfer, J.M., Ivy-Ochs, S., Wieler, R., Leya, I., Baur, H., Denton, G.H. and Schlücter, C., 1999. Cosmogenic noble gas studies in the oldest landscape on earth: surface

exposure ages of the Dry Valleys, Antarctica. Earth and Planetary Science Letters 167, 215-226.

Schaefer, J.M., Denton, G.H., Barrell, D.J.A., Ivy-Ochs, S., Kubik, P.W., Andersen, B.G., Phillips, F.M., Lowell, T.V. and Schlüchter, C., 2006. Near-Synchronous Interhemispheric Termination of the Last Glacial Maximum in Mid-Latitudes. Science 312, 1510-1513.

Seltzer, G.O., Rodbell, D.T., Baker, P.A., Fritz, S.C., Tapia, P.M., Rowe, H.D. and Dunbar, R.B., 2002. Early warming of tropical South America at the last glacial-interglacial transition. Science 296, 1685-1685.

Senanayake, W. E. and McElhinny, M.W., 1982. The effects of heating on low-temperature hysteresis and susceptibility properties of basalts. Physics of the Earth and Planetary Interiors 30, 317–321.

Smith, J.A., Seltzer, G.O. Farber, D.L., Rodbell, D.T. and Finkel, R.C., 2005a. Early local Last Glacial Maximum in the tropical Andes. Science 308, 678-681.

Smith, J.A., Finkel, R.C., Farber, D.L., Rodbell, D.T. and Seltzer, G.O., 2005b. Moraine preservation and boulder erosion in the tropical Andes: interpreting old surface exposure ages in glaciated valleys. Journal of Quaternary Science 20, 735-758.

Smith, J.A., Mark, B.G. and Rodbell, D.T., 2008. The timing and magnitude of mountain glaciation in the tropical Andes. Journal of Quaternary Science 23, 609-634.

Stone, J.O., 2000. Air pressure and cosmogenic isotope production. Journal of Geophysical Research, 105, 23 753-23 759.

Thompson, L.G., Mosley-Thompson, E., Davis, M.E., Lin, P.-N., Henderson, K.A., Cole-Dai, J., Bolzan, J.F. and Liu, K.-B., 1995. Late Glacial Stage and Holocene ice core records from Huascarán, Peru. Science 269, 46-50.

Thompson, L.G., Davis, M.E., Mosley-Thompson, E., Sowers, A., Henderson, K.A., Zagorodnov, V.S., Lin, P.-N., Mikhalenko, V.N., Campen, R.K., Bolzan, J.F., Cole-Dai, J. and Francou, B., 1998. A 25,000-Year Tropical Climate History from Bolivian Ice Cores. Science 282, 1858 – 1864.

Venturelli G., Fragipane M., Weibel M. and Antiga D, 1978. Trace element distribution in the Cainozoic lavas of Nevado Coropuna and Andagua Valley, Central Andes of southern Peru. Bulletin of Volcanology 41, 213-228.

Winckler, G., Anderson, R.F. and Schlosser, P., 2005. Equatorial Pacific productivity and dust flux during the Mid-Pleistocene climate transition. Paleoceanography 20(4): PA4025, 10.1029/2005PA001177.

Zech, R., Kull, Ch., Kubik, P.W. and Veit, H, 2007. LGM and Late Glacial glacier advances in the Cordillera Real and Cochabamba (Bolivia) deduced from 10Be surface exposure dating. Climate of the Past 3, 623-635.

Zech, R., May, J-H., Kull, C., Ilgner, J., Kubik, P.W. and Veit, H, 2008. Timing of the late Quaternary glaciation in the Andes from ~15 to 40ºS. Journal of Quaternary Science 23, 635-647.

Appendix

Methodology and geographical context of the Junin-Cordillera Real glacier record

Smith et al. (2005a,b) presented a glacial chronology for the Junin Valleys, central Peru, and the Milluni and Zongo Valleys, Bolivia, constrained by 106 ^{10}Be ages. These ages were recalculated using the CRONUS online calculator and published by Smith et al. (2008). On the basis of moraine position, geomorphic "character", and surface-exposure ages, deposits were grouped into four age populations – A to D. The oldest moraines, Group D, occur in the lowest reaches of the Junin Valleys and on the edge of the Junin Plain and are believed to predate the last glacial cycle (Smith et al., 2005a,b). Deposits corresponding to the 'local last glacial maximum' (LLGM) – Group C – typically occupy mid-valley positions in the Junin Valleys. Twenty-two recalculated ^{10}Be ages from these moraines, ranging from 17.0 to 46.4 ka (minus one outlier – PE02-COL-05), have a mean age of 26.9 ka. Group C is represented in Milluni Valley by three lateral moraines, two of which have been dated to between 15.5 and 34.2 ka (Table S1 in Smith et al., 2005a), with a mean age of 25.8 ka. No Group C deposits were found in Zongo Valley.

Moraine Group B is described as occurring 1-2 km up-valley of the LLGM moraines in the Junin Valleys. Contrary to this, however, Fig. S1 (in Smith et al., 2005a) shows that the Alcacocha Glacier was just as extensive during Group B time as during the LLGM. Thirty-four recalculated ages (with the omission of sample PE01-ALC-07) from the western Junin Valleys constrain deposition of this group to between 13.9 and 2.7 ka and produce a mean age of 16.1 ± 1.5 ka. Group B moraines in Milluni Valley are located more than 10 km up-valley of the LLGM terminus (Fig. 2, Smith et al, 2005a) and have a mean age (recalculated) of 11.1 ± 3.4 ka. In Zongo Valley, moraines of the same group form the outermost glacial deposits and are located more than 1000 m lower in elevation than Group B deposits in Milluni Valley. Nine recalculated ages from the Zongo Valley moraines (samples Zong-03-08, Zong-03-10, and Zong-03-11 were discarded as young outliers) range from 7.5 to 18.0 ka and have a mean age of 13.9 ± 3.1 ka. Group A moraines have been documented only in Alcacocha Valley, where six recalculated ^{10}Be

ages falling between 11.8 and 17.1 ka (AL004 is omitted by the authors as an old outlier) have a mean age of 14.3 ± 1.9 ka, and in Zongo Valley, where twelve ages range from 11.1 to 16.6 ka and have a mean age of 13.2 ± 1.6 ka. The mean (recalculated) age of all Group A samples is 13.6 ± 1.7 ka.

All surface-exposure ages published in Smith et al. (2005a) were calculated using the production rate of Nishiizumi et al. (1989) and corrected according to Stone (2000), with scaling according to Lal (1991). Geomagnetic corrections were made according to Senanayake and McElhinny (1982) and Ohno and Hamano (1992). The recalculated ages shown here for comparison to our Coropuna data (Appendix Table 3) are from the Alcacocha and Antacocha Valleys and were produced by Smith et al. (2008) using the global ^{10}Be production rate data set and four currently accepted scaling protocols as summarised in Balco et al. (2008). We concentrated on the Junin data because they show the highest internal consistency.

Methodology and geographical context of the Cordillera Blanca glacier record

Farber et al. (2005) presented a ^{10}Be dataset from moraines in Quebrada Cojup and Quebrada Llaca in the Cordillera Blanca, Peru. Of these, thirteen ages constrain the Rurec (Rodbell, 1993) moraines and twelve ages constrain the Laguna Baja moraines (Rodbell, 1993), interpreted as representing the LGM and a deglacial readvance/stillstand, respectively. Recalculated using the CRONUS online calculator and the Lm scaling scheme (Balco et al., 2008), ages from the Rurec moraines range from 16.4 to 27.9 ka BP, with a mean age of 19.9 ± 1.9 ka BP (Appendix Table 4). Recalculated ages from the Laguna Baja moraines range from 11.9 to 18.6 ka BP and give a mean age of 14.7 ± 0.9 ka BP (Appendix Table 4). Farber et al. (2005) present an additional sixteen ages from older moraines – the Cojup moraines – located down-valley of the Rurec limits. These range from 118 to 441 ka BP (Table 3, Farber et al., 2005).

Surface-exposure ages published in Farber et al. (2005) were calculated using a production rate of 5.44 atoms/g/yr (based on Nishiizumi et al. (1989) and Clark and Gillespie (1997)), scaled according to Lal (1991) and Stone (2000), and corrected for local atmospheric effects. Geomagnetic corrections were made using the Nishiizumi et al. (1989) correction scheme, modified according to the records of Guyodo and Valet (1999), McElhinny and Senanayake (1982), and Ohno and Hamano (1992).

Methodology and geographical context of the Mauna Kea (Hawaii) glacier record

The Hawaiian glacial record presented by Blard et al. (2007) is based upon cosmogenic ^{3}He ages from Late-Pleistocene moraines in Pohakuloa Gulch, Mauna Kea. All surface-exposure ages reported by Blard et al. (2007) were calculated using a production rate of 128 ± 5 atoms/g/yr (Blard et al., 2006), as well as the scaling coefficients of Stone (2000), the geomagnetic corrections of Dunai (2000), and the dipole database of Carcaillet et al. (2004). In addition, the authors corrected for an estimated constant subsidence rate of 2.6 ± 0.4 mm/ka for Hawaii. For comparison with our Coropuna data, we recalculated the Hawaiian ^{3}He ages using the same production rate and scaling parameters described in Section 3.4.

Figure Captions

Figure 1 (a). Map of Peru showing location of Nevado Coropuna (NC), Lago Junin (LJ), the Cordillera Blanca (CB), and the Cordillera Real (CR), Bolivia. (b) Locations of sites mentioned in text and lava flows (black) on Nevado Coropuna (NC). Quebrada Ullullo (QU); Quebrada Santiago (QS); Queña Ranra (QR); Quebrada Sigue Chico (QSC); Lago Pallar Cocha (LPC); Quebrada Huayllaura (QH). **C-I** moraines are shown as black lines and **C-II** moraines as red lines. Dashed box represents area shown in Figure 2.

Figure 2. Geomorphic map of Quebradas Ullullo and Santiago and Queña Ranra, showing glacial deposits, glacier ice, and other surfaces. Surface-exposure ages correspond to Table 2. Asterisks denote ages from LGM drift edge that we speculate are younger than landform's true age.

Figure 3. Locations of all surface-exposure ages calculated using Lm scaling. Italics denote outlier. Asterisks denote ages from LGM drift edge that we speculate are younger than landform's true age. **C-I** drift shown as pink and moraines as black, **C-II** moraines as red. Older (pre-**C-I**) glacial deposits are shown in green and brown.

Figure 4. Boulder (NC10) located on the crest of the east lateral moraine in *Q*. Santiago. This boulder is typical of deposits at Nevado Coropuna in that it exhibits glacial moulding, polish and striations. The western lateral moraine of *Q*. Santiago is visible in the distance.

Figure 5. A: ^{3}He ages and probability curves from Coropuna. B and C: Recalculated ^{10}Be ages and probability curves from Group A and B moraines, Junin Valleys (Smith et al., 2008), and from the Rurec and Laguna Baja moraines, Cordillera Blanca (Farber et al., 2005). All ages shown were calculated using the CRONUS online calculator and the scaling schemes described in Balco et al. (2008).

Table 1. Nevado Coropuna sample details and measured ^{3}He concentrations.

Table 2. Coropuna surface-exposure ages calculated using the Li and Lm scaling schemes (Balco et al., 2008). Italics denote outlier. Mean ages do not include outliers.

Appendix Table 1. Helium isotope data of all pyroxene samples. Errors include statistical and mass spectrometer stability uncertainties. Errors due to the calibration gas concentration are not included but should be on the order of 2%. Analyses were controlled by repeated measurement of the 'CRONUS-Earth pyroxene intercomparison material'. ^{3}He/^{4}He ratios are given as measured and relative to the atmospheric ^{3}He/^{4}He value R_a=1.384 x 10^{-6}. Italics denote outlier. Correction for non-cosmogenic ^{3}He was not necessary for this dataset: with ^{3}He/^{4}He ratios ranging from 2-85 times the atmospheric ratio, a simple estimate based on the measured ^{4}He concentrations and a conservative high non-cosmogenic ^{3}He/^{4}He ratio for the investigated rocks yields 'corrections' of less than 1% even for the sample with the lowest 3He/4He ratio (NC13).

Appendix Table 2. Nevado Coropuna ^{3}He ages calculated using the CRONUS online calculator and the four currently accepted scaling schemes (Balco et al., 2008). All calculations include a correction for geomagnetic flux. Also shown are the actual production rates (sea level–high latitude) used to make the calculations.

Appendix Table 3. ^{10}Be ages from Junin Valleys, central Peru, recalculated using the CRONUS online calculator and scaling schemes described by Balco et al. (2008). Also shown are the actual production rates used in the recalculations. Original data were calculated by Smith et al. (2005a) using production rates of Nishiizumi et al. (1989), with Stone (2000) correction and Lal's (1991) scaling, and were corrected for magnetic flux according to Senanayake and McElhinny (1982) and Ohno and Hamono (1992). The dataset was recalculated by Smith et al. (2005b) using a revised production rate of 5.44 at/g/yr.

Appendix Table 4. ^{10}Be ages from the Cordillera Blanca, central Peru, recalculated using the CRONUS online calculator and scaling schemes described by Balco et al. (2008). Shown are the actual production rates used in the recalculations. Original data were calculated by Farber et al. (2005) using production rates based on Nishiizumi et al. (1989) and Clark and Gillespie (1997), scaled according to Lal (1991) and Stone (2000), corrected for magnetic flux according to Senanayake and McElhinny (1982), Ohno and Hamono (1992), and Guyodo and Valet (1999).

Appendix Table 5.
^{3}He ages from Mauna Kea, Hawaii, recalculated using the Balco et al. (2008) protocol modified for ^{3}He measurements (Goehring et al., in prep). Also shown are the actual production rates used to make the calculations. Original data were calculated by Blard et al. (2007) using production rate of Blard et al. (2006), the scaling protocol of Stone (2000), and corrections for geomagnetic flux according to Dunai (2001) and Carcaillet et al. (2004). Asterisks denote weighted means for single boulder or cobble samples (MK 12C from two replicates, MK 9D and MK 11 from two phenocryst types).

Figure 1a/1b

Click here to download high resolution image

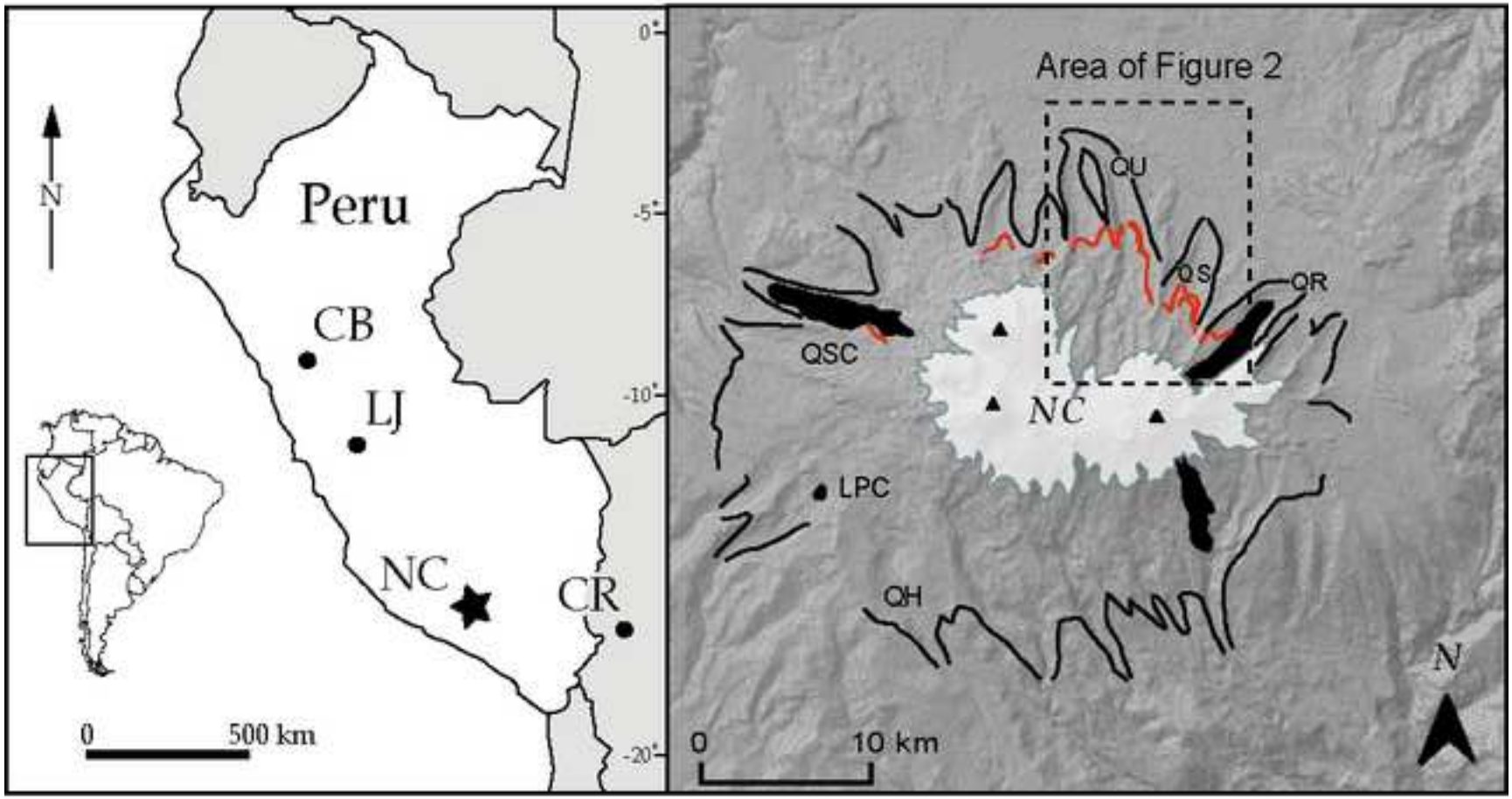

Figure 2

Click here to download high resolution image

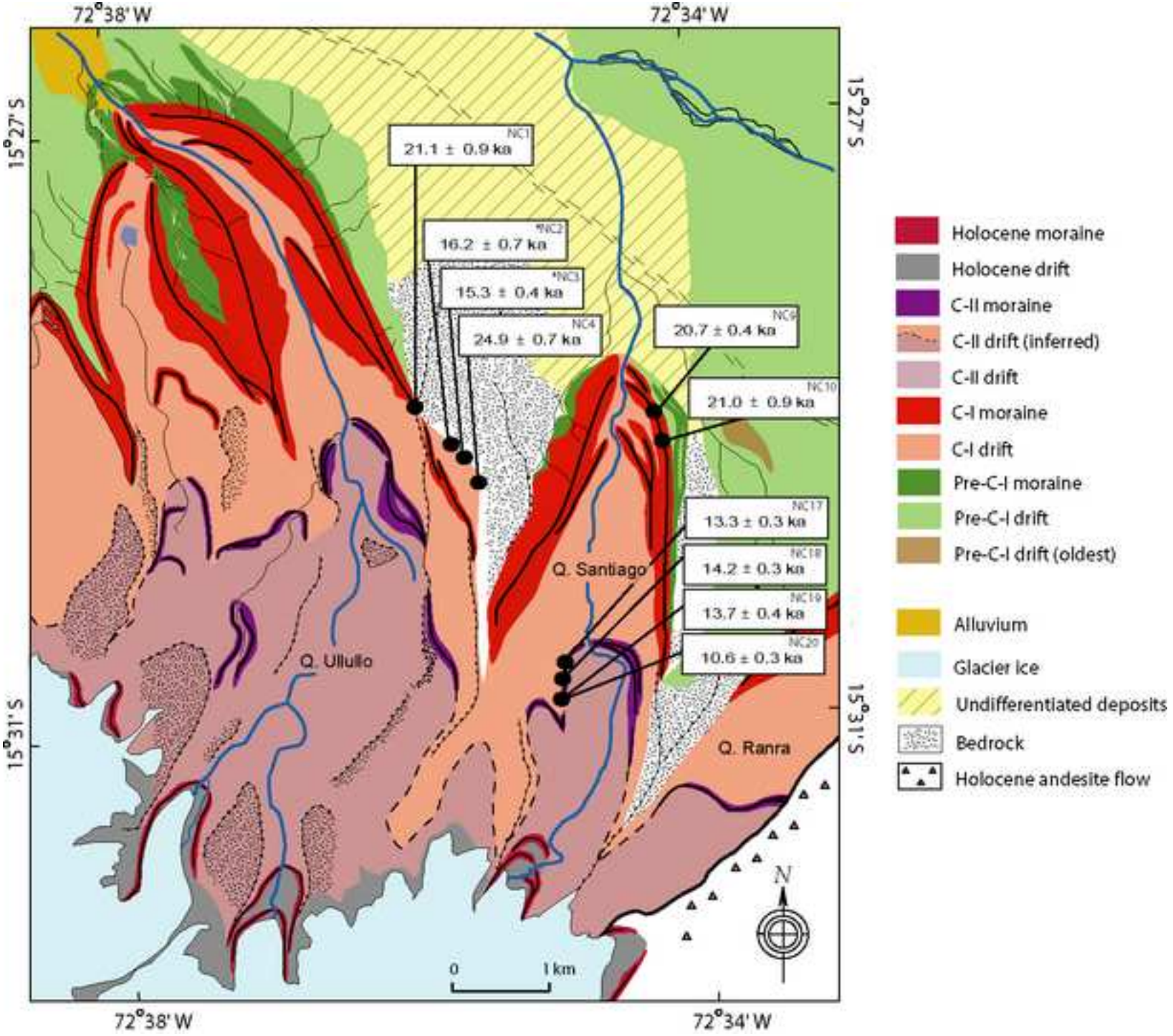

Figure 3

Click here to download high resolution image

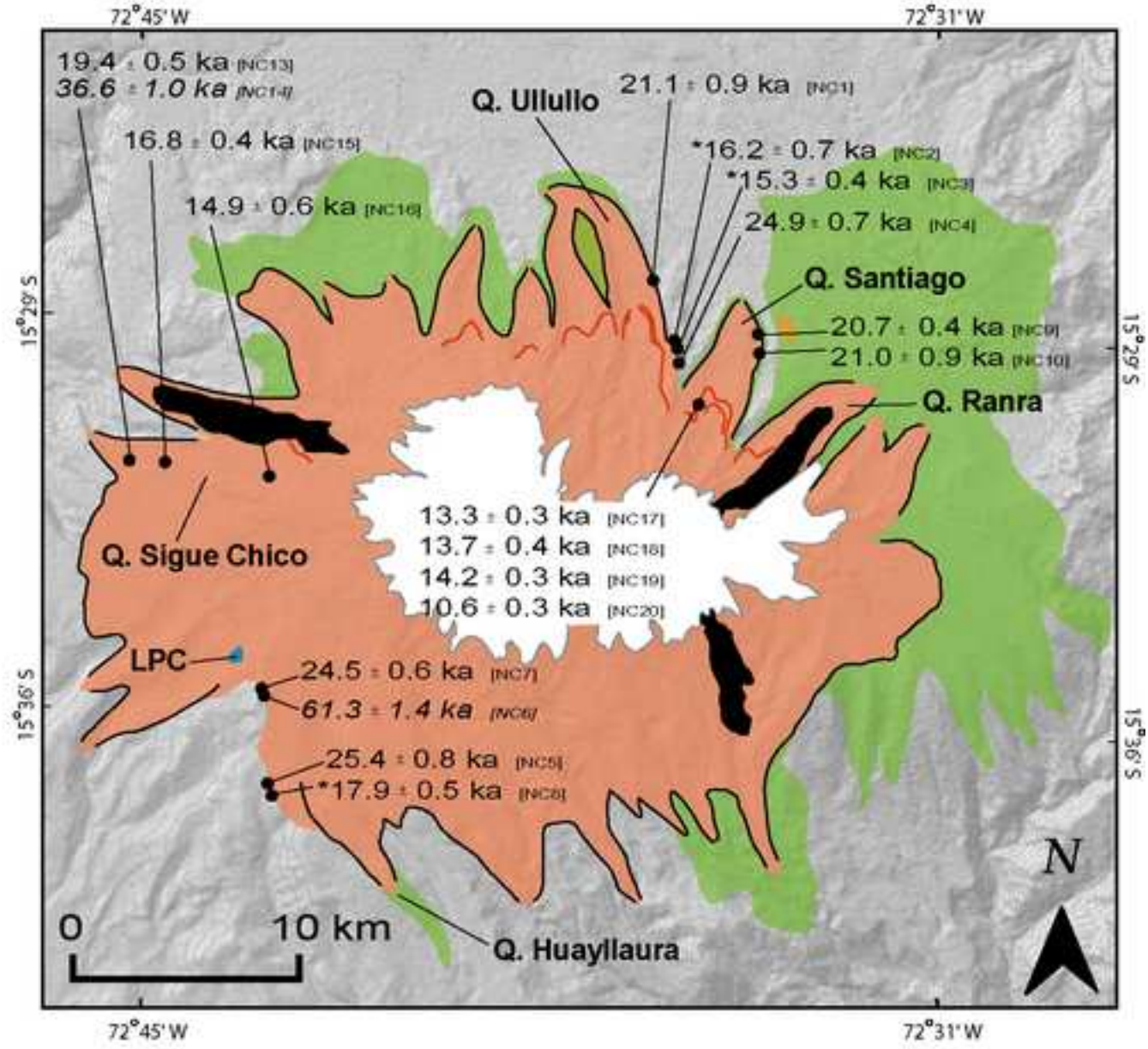

Figure 4

Click here to download high resolution image

Figure 5

Click here to download high resolution image

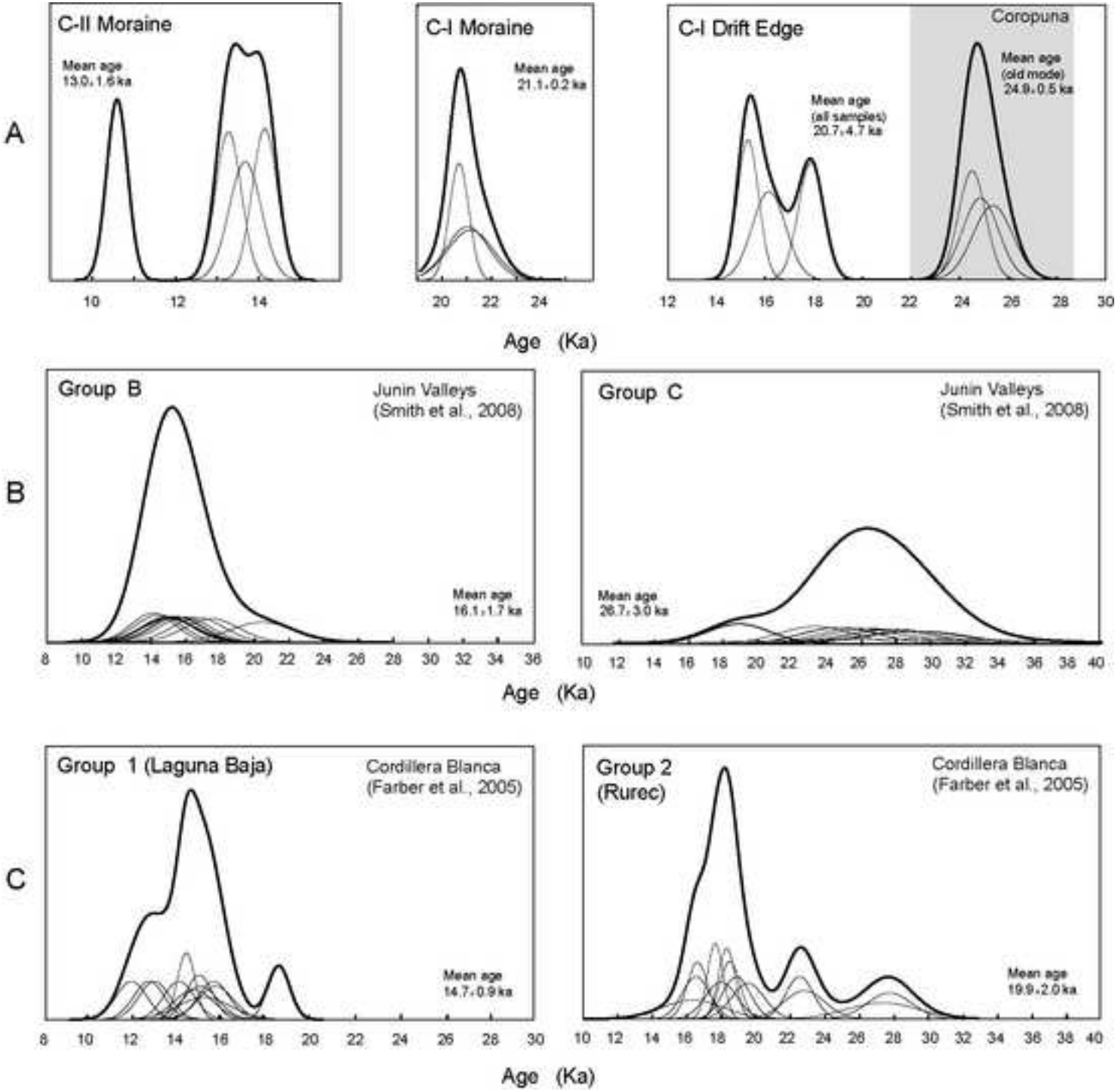

Table 1

Table 1. Nevado Coropuna sample details and measured ^{3}He concentrations.

Sample No.	Lat. S	Long. W	altitude	air pressure	type	thickness (cm)	density (g/cm^3)	shielding	erosion (mm/yr)	$^{3}He_{cos}$ (atoms/g)	1 sigma
C-I drift edge											
NC2	15º29.190’	72º35.775’	5016	556	cobble	6.0	2.7	1.000	0	2.240×10^{7}	9.580×10^{5}
NC3	15º29.218’	72º35.706’	5018	555	cobble	5.5	2.7	1.000	0	2.127×10^{7}	6.055×10^{5}
NC4	15º29.230’	72º35.645’	5023	555	cobble	4.0	2.7	0.999	0	3.747×10^{7}	1.130×10^{6}
NC5	15º36.484’	72º43.408’	4798	571	cobble	2.0	2.7	1.000	0	3.547×10^{7}	1.154×10^{6}
NC6	15º35.275’	72º43.088’	4880	571	cobble	2.0	2.7	1.000	0	9.618×10^{7}	2.287×10^{6}
NC7	15º35.275’	72º43.088’	4880	565	cobble	2.0	2.7	1.000	0	3.536×10^{7}	8.172×10^{5}
NC8	15º36.531’	72º43.371’	4795	565	cobble	5.0	2.7	1.000	0	2.406×10^{7}	7.001×10^{5}
C-I moraine											
NC1	15º29.917’	72º36.001’	4971	559	cobble	3.3	2.7	1.000	0	3.044×10^{7}	1.323×10^{6}
NC9	15º29.247’	72º34.365’	4844	568	boulder	2.0	2.7	1.000	0	2.844×10^{7}	9.740×10^{5}
NC10	15º29.682’	72º34.415’	4936	568	boulder	2.8	2.7	1.000	0	2.876×10^{7}	1.185×10^{6}
Recessional											
NC13	15º31.424’	72º45.305’	4606	585	cobble	4.0	2.7	1.000	0	2.350×10^{7}	5.738×10^{5}
NC15	15º31.399’	72º44.797’	4641	582	cobble	2.0	2.7	1.000	0	2.968×10^{7}	4.928×10^{5}
NC16	15º31.620’	72º42.967’	4899	564	cobble	4.0	2.7	1.000	0	1.983×10^{7}	7.350×10^{5}
C-II moraine											
NC17	15º30.653’	72º35.159’	5082	551	cobble	6.3	2.7	1.000	0	1.862×10^{7}	4.351×10^{5}
NC18	15º30.660’	72º35.172’	5087	551	cobble	7.0	2.7	1.000	0	1.977×10^{7}	4.229×10^{5}
NC19	15º30.684’	72º35.174’	5080	551	cobble	6.0	2.7	1.000	0	1.924×10^{7}	5.464×10^{5}
NC20	15º30.696’	72º35.167’	5089	551	cobble	6.0	2.7	1.000	0	1.493×10^{7}	3.589×10^{5}

Table 2

Table 2. Coropuna surface-exposure ages calculated using the Li and Lm scaling schemes (Balco et al., 2008). Italics denote outlier. Mean ages do not include outliers.

Sample No.	Li (ka)	Lm (ka)
Production rate (at/g/yr**)**	131 ± 6	117 ± 6
C-I drift edge		
NC2	12.99 ± 0.6	16.15 ± 0.7
NC3	12.18 ± 0.3	15.29 ± 0.4
NC4	20.44 ± 0.6	24.85 ± 0.7
NC5	21.15 ± 0.7	25.36 ± 0.8
NC6	*46.86 ± 1.1*	*61.34 ± 1.4*
NC7	20.31 ± 0.5	24.50 ± 0.6
NC8	14.66 ± 0.4	17.88 ± 0.5
Age Ranges	**12.2 – 21.2**	**15.29 – 25.36**
Mean Age	16.96 ± 4.1	20.67 ± 4.7
C-I moraine		
NC1	17.25 ± 0.8	21.14 ± 0.9
NC9	17.0 ± 0.3	20.68 ± 0.4
NC10	17.28 ± 0.7	21.03 ± 0.9
Age Ranges	**17.0 – 17.28**	**20.68 – 21.14**
Mean Age	17.18 ± 0.2	20.95 ± 0.2
Recessional		
NC13	16.18 ± 0.4	19.39 ± 0.5
NC14	*31.19 ± 0.8*	*36.55 ± 1.0*
NC15	13.89 ± 0.4	16.76 ± 0.4
NC16	11.91 ± 0.4	14.89 ± 0.6
C-II moraine		
NC17	10.36 ± 0.2	13.27 ± 0.3
NC18	11.08 ± 0.2	14.15 ± 0.3
NC19	10.69 ± 0.3	13.68 ± 0.4
NC20	8.12 ± 0.2	10.59 ± 0.3
Age Ranges	**8.12 – 11.08**	**10.59 – 14.15**
Mean Age	10.06 ± 1.3	12.92 ± 1.6

Appendix Table 1

Appendix Table 1. Helium isotope data of all pyroxene samples. Errors include statistical and mass spectrometer stability uncertainties. Errors due to the calibration gas concentration are not included but should be on the order of 2%. Analyses were controlled by repeated measurement of the 'CRONUS-Earth pyroxene intercomparison material'. $^{3}He/^{4}He$ ratios are given as measured and relative to the atmospheric $^{3}He/^{4}He$ value R_a=1.384 x 10^{-6}. Italics denote outlier. Correction for non-cosmogenic ^{3}He was not necessary for this dataset: with $^{3}He/^{4}He$ ratios ranging from 2-85 times the atmospheric ratio, a simple estimate based on the measured ^{4}He concentrations and a conservative high non-cosmogenic $^{3}He/^{4}He$ ratio for the investigated rocks yields 'corrections' of less than 1% even for the sample with the lowest 3He/4He ratio (NC13).

Sample No.	$^{3}He/^{4}He$	1 sigma	$^{3}He/^{4}He$ (R/R_a)	^{4}He (atoms/g)	1 sigma (atoms/g)	^{3}He (atoms/g)	1 sigma (atoms/g)
C-I drift edge							
NC2	1.720×10^{-5}	8.604×10^{-7}	12	1.303×10^{12}	3.373×10^{10}	2.240×10^{7}	9.580×10^{5}
NC3	6.194×10^{-5}	2.743×10^{-6}	45	3.434×10^{11}	1.162×10^{10}	2.127×10^{7}	6.055×10^{5}
NC4	1.040×10^{-4}	3.408×10^{-6}	75	3.601×10^{11}	4.596×10^{9}	3.747×10^{7}	1.130×10^{6}
NC5	1.172×10^{-4}	4.963×10^{-6}	85	3.028×10^{11}	8.215×10^{9}	3.547×10^{7}	1.154×10^{6}
NC6	7.970×10^{-5}	1.975×10^{-6}	58	1.207×10^{12}	8.437×10^{9}	9.618×10^{7}	2.287×10^{6}
NC7	2.093×10^{-5}	5.038×10^{-7}	15	1.690×10^{12}	1.138×10^{10}	3.536×10^{7}	8.172×10^{5}
NC8	2.085×10^{-5}	7.053×10^{-7}	15	1.154×10^{12}	1.974×10^{10}	2.406×10^{7}	7.001×10^{5}
C-I moraine							
NC1	1.066×10^{-4}	7.777×10^{-6}	77	2.856×10^{11}	1.672×10^{10}	3.044×10^{7}	1.323×10^{6}
NC9	4.076×10^{-5}	1.416×10^{-6}	29	6.978×10^{11}	4.088×10^{9}	2.844×10^{7}	9.740×10^{5}
NC10	3.574×10^{-5}	1.514×10^{-6}	26	8.049×10^{11}	7.948×10^{9}	2.876×10^{7}	1.185×10^{6}
Recessional							
NC13	2.672×10^{-6}	7.508×10^{-8}	2	8.793×10^{12}	1.205×10^{11}	2.350×10^{7}	5.738×10^{5}
NC15	4.379×10^{-5}	1.227×10^{-6}	32	4.723×10^{11}	7.933×10^{9}	2.068×10^{7}	4.928×10^{5}
NC16	5.766×10^{-5}	3.608×10^{-6}	42	3.438×10^{11}	1.732×10^{10}	1.983×10^{7}	7.350×10^{5}
C-II moraine							
NC17	1.571×10^{-5}	4.729×10^{-7}	11	1.185×10^{12}	2.232×10^{10}	1.862×10^{7}	4.351×10^{5}
NC18	1.738×10^{-5}	1.782×10^{-7}	13	1.138×10^{12}	1.952×10^{10}	1.977×10^{7}	4.229×10^{5}
NC19	1.845×10^{-5}	6.204×10^{-7}	13	1.043×10^{12}	1.864×10^{10}	1.924×10^{7}	5.464×10^{5}
NC20	1.343×10^{-5}	3.978×10^{7}	10	1.112×10^{12}	1.911×10^{10}	1.493×10^{7}	3.589×10^{5}

Appendix Table 2

Appendix Table 2. Nevado Coropuna ^{3}He ages calculated using the CRONUS online calculator and the four currently accepted scaling schemes (Balco et al., 2008). All calculations include a correction for geomagnetic flux. Also shown are the actual production rates (sea level–high latitude) used to make the calculations

Sample No.	De (ka)	Du (ka)	Li (ka)	Lm (ka)
Production rate (atoms/g/yr)	123 ± 6	123 ± 6	131 ± 6	117 ± 6
C-I drift edge				
NC2	12.68 ± 0.5	13.03 ± 0.6	12.99 ± 0.6	16.15 ± 0.7
NC3	11.88 ± 0.3	12.19 ± 0.4	12.18 ± 0.3	15.29 ± 0.4
NC4	20.11 ± 0.6	20.95 ± 0.6	20.44 ± 0.6	24.85 ± 0.7
NC5	20.79 ± 0.7	21.71 ± 0.7	21.15 ± 0.7	25.36 ± 0.8
NC6	*46.72 ± 1.1*	*49.25 ± 1.2*	*48.86 ± 1.1*	*61.34 ± 1.4*
NC7	19.69 ± 0.5	20.82 ± 0.5	20.31 ± 0.4	24.5 ± 0.6
NC8	14.34 ± 0.4	14.77 ± 0.4	14.66 ± 0.4	17.88 ± 0.5
Age Range	**11.88 – 20.79**	**12.19 – 21.71**	**12.18 – 21.15**	**15.29 – 25.36**
Mean Age	16.63 ± 4.1	17.24 ± 4.4	16.96 ± 4.1	20.67 ± 4.7
C-1 moraine				
NC1	16.93 ± 0.7	17.53 ± 0.8	17.25 ± 0.8	21.14 ± 0.9
NC9	16.67 ± 0.3	17.27 ± 0.3	17.0 ± 0.3	20.68 ± 0.4
NC10	16.95 ± 0.7	17.57 ± 0.7	17.28 ± 0.7	21.03 ± 0.9
Age Range	**16.67 – 16.95**	**17.27 – 17.57**	**17.0 – 17.28**	**20.68 – 21.14**
Mean Age	16.85 ± 0.2	17.46 ± 0.2	17.18 ± 0.2	20.95 ± 0.2
Recessional				
NC13	15.83 ± 0.4	16.39 ± 0.4	16.18 ± 0.4	19.39 ± 0.5
NC15	13.54 ± 0.4	13.98 ± 0.4	13.89 ± 0.4	16.76 ± 0.4
NC16	11.61 ± 0.4	11.94 ± 0.4	11.91 ± 0.4	14.89 ± 0.6
C-II moraine				
NC17	10.11 ± 0.2	10.35 ± 0.2	10.36 ± 0.2	13.27 ± 0.3
NC18	10.82 ± 0.2	11.09 ± 0.2	11.08 ± 0.2	14.15 ± 0.3
NC19	10.43 ± 0.3	10.69 ± 0.3	10.69 ± 0.3	13.68 ± 0.4
NC20	7.91 ± 0.2	8.11 ± 0.2	8.12 ± 0.2	10.59 ± 0.3
Age Range	**7.91 – 10.82**	**8.11 – 11.09**	**8.12 – 11.08**	**10.59 – 14.15**
Mean Age	9.81 ± 1.3	10.06 ± 1.3	10.06 ± 1.3	12.92 ± 1.6

Appendix Table 3

Appendix Table 3. ^{10}Be ages from Junin Valleys, central Peru, recalculated using the CRONUS online calculator and scaling schemes described by Balco et al. (2008). Also shown are the actual production rates used in the recalculations. Original data were calculated by Smith et al. (2005a) using production rates of Nishiizumi et al. (1989), with Stone (2000) correction and Lal's (1991) scaling, and were corrected for magnetic flux according to Senanayake and McElhinny (1982) and Ohno and Hamono (1992). The dataset was recalculated by Smith et al. (2005b) using a revised production rate of 5.44 at/g/yr.

Sample No.	De (ka)	Du (ka)	Li (ka)	Lm (ka)	Smith et al. (2005a) published age (ka)
Production rate (atoms/g/yr)	4.88 ± 0.6	4.9 ± 0.6	5.39 ± 0.5	4.84 ± 0.4	5.06 ± 0.3
Junin Valleys Group C					
PE01-ALC-26	16.43 ± 0.7	17.13 ± 0.8	16.78 ± 0.8	19.22 ± 0.9	21.11 ± 0.9
PE01-ALC-27	25.94 ± 1.1	27.45 ± 1.2	26.42 ± 1.2	29.77 ± 1.3	33.63 ± 1.6
PE01-ALC-28	25.55 ± 1.2	27.05 ± 1.2	26.03 ± 1.2	29.35 ± 1.3	33.19 ± 1.6
PE01-ALC-29	25.69 ± 1.2	27.2 ± 1.3	26.18 ± 1.3	29.51 ± 1.4	33.36 ± 1.7
PE01-ANT-08	21.87 ± 0.6	23.01 ± 0.6	22.31 ± 0.6	25.13 ± 0.7	28.02 ± 0.7
PE01-ANT-09	21.97 ± 0.5	23.11 ± 0.6	22.41 ± 0.6	25.24 ± 0.7	28.21 ± 0.7
PE01-ANT-10	22.89 ± 0.5	24.12 ± 0.6	23.34 ± 0.6	26.3 ± 0.7	29.46 ± 0.7
PE01-ANT-11	24.8 ± 0.5	26.27 ± 0.6	25.29 ± 0.6	28.39 ± 0.7	31.99 ± 0.9
PE01-ANT-12	24.29 ± 0.6	25.71 ± 0.6	24.77 ± 0.6	27.87 ± 0.7	31.33 ± 0.8
PE01-ANT-13	23.47 ± 0.6	24.78 ± 0.6	23.92 ± 0.6	26.97 ± 0.7	30.23 ± 0.7
PE01-ANT-14	20.63 ± 0.4	21.7 ± 0.4	21.08 ± 0.4	23.73 ± 0.5	26.51 ± 0.7
PE01-ANT-15	24.98 ± 0.6	26.46 ± 0.6	25.48 ± 0.6	28.58 ± 0.7	32.33 ± 0.8
Age Range	**16.43 – 25.94**	**17.13 – 27.45**	**16.78 – 26.42**	**19.22 – 29.77**	**21.11 – 33.63**
Mean Age	23.21 ± 2.7	24.5 ± 2.9	23.67 ± 2.7	26.67 ± 3.0	29.94 ± 3.6
Junin Valleys Group B					
AL006	15.13 ± 0.4	15.72 ± 0.4	15.45 ± 0.4	17.7 ± 0.5	19.67 ± 0.4
AL007	11.99 ± 0.3	12.43 ± 0.3	12.25 ± 0.3	14.31 ± 0.4	15.86 ± 0.4
AL010	14.42 ± 0.4	14.97 ± 0.4	14.74 ± 0.4	16.91 ± 0.4	18.89 ± 0.4
PE01-ALC-03	13.2 ± 0.5	13.69 ± 0.5	13.5 ± 0.5	15.6 ± 0.5	16.71 ± 0.5
PE01-ALC-04	13.71 ± 0.5	14.22 ± 0.5	14.03 ± 0.5	16.14 ± 0.5	17.36 ± 0.5
PE01-ALC-05	17.65 ± 0.5	18.47 ± 0.5	18.03 ± 0.5	20.66 ± 0.6	22.71 ± 0.6
PE01-ALC-06	13.38 ± 0.5	13.88 ± 0.5	13.69 ± 0.5	15.79 ± 0.6	16.94 ± 0.5
PE01-ALC-23	12.9 ± 0.5	13.37 ± 0.6	13.19 ± 0.6	15.26 ± 0.6	16.33 ± 0.6
PE01-ALC-24	12.79 ± 0.7	13.26 ± 0.8	13.08 ± 0.7	15.15 ± 0.9	16.21 ± 0.9
PE01-ALC-25	12.76 ± 0.5	13.23 ± 0.6	13.05 ± 0.6	15.11 ± 0.6	16.17 ± 0.6
PE02-ALC-01	12.93 ± 0.7	13.4 ± 0.8	13.22 ± 0.8	15.3 ± 0.6	16.4 ± 0.9
PE02-ALC-05	12.29 ± 0.4	12.75 ± 0.4	12.57 ± 0.4	14.63 ± 0.9	15.64 ± 0.5
Age Range	**11.99 – 17.65**	**12.43 – 18.47**	**12.25 – 18.03**	**14.31 – 20.66**	**15.86 – 22.71**
Mean Age	13.6 ± 1.5	14.12 ± 1.6	13.9 ± 1.5	16.05 ± 1.7	17.4 ± 2.0

Appendix Table 4

Appendix Table 4. ^{10}Be ages from the Cordillera Blanca, central Peru, recalculated using the CRONUS online calculator and scaling schemes described by Balco et al. (2008). Shown are the actual production rates used in the recalculations. Original data were calculated by Farber et al. (2005) using production rates based on Nishiizumi et al. (1989) and Clark and Gillespie (1997), scaled according to Lal (1991) and Stone (2000), corrected for magnetic flux according to Senanayake and McElhinny (1982), Ohno and Hamono (1992), and Guyodo and Valet (1999).

Sample No.	De (ka)	Du (ka)	Li (ka)	Lm (ka)	Farber et al. (2005) published age (ka)
Production rate (atoms/g/yr)	4.88 ± 0.6	4.9 ± 0.6	5.39 ± 0.5	4.84 ± 0.4	5.44
Rurec moraines					
HU-1	16.11 ± 0.6	16.86 ± 0.6	16.58 ± 0.6	18.55 ± 0.6	19.24 ± 0.6
HU-2	15.39 ± 0.5	16.09 ± 0.5	15.84 ± 0.5	17.71 ± 0.5	18.24 ± 0.4
HU-4	15.99 ± 0.5	16.74 ± 0.5	16.46 ± 0.5	18.38 ± 0.5	19.05 ± 0.5
K-I	23.94 ± 2.1	25.43 ± 2.1	24.62 ± 2.1	27.04 ± 2.1	28.41 ± 1.9
K-2	14.37 ± 1.7	14.99 ± 1.7	14.81 ± 1.7	16.38 ± 1.7	16.73 ± 1.7
K-3	17.32 ± 0.9	18.18 ± 0.9	17.84 ± 0.9	19.61 ± 0.9	20.33 ± 0.9
K-4	15.84 ± 0.9	16.57 ± 0.9	16.31 ± 0.9	18.05 ± 0.9	18.62 ± 0.9
K-5a	20.15 ± 1.2	21.28 ± 1.2	20.76 ± 1.2	22.9 ± 1.2	23.61 ± 0.7
K-5b	19.89 ± 0.8	21.01 ± 0.8	20.49 ± 0.8	22.63 ± 0.8	23.92 ± 1.1
K-7	14.37 ± 0.8	15.00 ± 0.8	14.81 ± 0.8	16.58 ± 0.8	16.98 ± 0.8
K-10	24.76 ± 1.3	26.32 ± 1.3	25.46 ± 1.3	27.87 ± 1.3	29.33 ± 1.2
Peru-18	14.70 ± 0.6	15.34 ± 0.6	15.15 ± 0.6	16.67 ± 0.6	17.04 ± 0.6
Peru-21	14.36 ± 0.8	14.98 ± 0.8	14.80 ± 0.8	16.39 ± 0.8	19.60 ± 0.7
Age Range	**14.36 – 24.76**	**14.98 – 26.32**	**14.80 – 25.46**	**16.38 – 27.87**	**16.73 – 29.33**
Mean Age	17.48 ± 1.8	18.37 ± 1.9	17.99 ± 1.8	19.90 ± 1.9	20.85 ± 2.1
Laguna Baja moraines					
GV-22	16.01 ± 0.5	16.73 ± 0.5	16.43 ± 0.5	18.62 ± 0.5	19.46 ± 0.5
GV-23	12.98 ± 1.2	13.52 ± 1.2	13.35 ± 1.2	15.24 ± 1.2	15.53 ± 1.1
GV-24	12.24 ± 0.4	12.75 ± 0.4	12.59 ± 0.4	14.43 ± 0.4	14.69 ± 3.5
K-13	12.24 ± 0.7	12.76 ± 0.7	12.61 ± 0.7	14.11 ± 0.7	14.23 ± 0.7
K-6a	12.94 ± 0.6	13.49 ± 3.7	13.33 ± 3.7	15.01 ± 3.8	15.24 ± 0.6
K-6b	12.99 ± 0.8	13.54 ± 3.6	13.38 ± 3.5	15.06 ± 3.8	15.28 ± 0.7
K-8a	13.61 ± 0.8	14.20 ± 0.8	14.03 ± 0.8	15.76 ± 0.8	16.07 ± 0.8
K-8b	13.52 ± 0.7	14.10 ± 4.8	13.94 ± 4.7	15.67 ± 5.1	15.97 ± 0.7
K-9	12.88 ± 0.9	13.42 ± 4.7	13.27 ± 4.6	14.77 ± 5.0	14.94 ± 0.8
P98GV-C19	10.01 ± 0.8	10.42 ± 4.8	10.24 ± 4.7	11.94 ± 5.1	11.94 ± 0.8
P98GV-C20	10.89 ± 0.4	11.34 ± 0.4	11.16 ± 0.4	12.98 ± 0.4	13.08 ± 0.3
P98GV-C21	10.68 ± 0.6	11.13 ± 0.6	10.94 ± 0.6	12.74 ± 0.6	12.83 ± 0.6
Age Range	**10.01 – 16.01**	**10.42 – 16.73**	**10.24 – 16.43**	**11.94 – 18.62**	**11.94 – 19.46**
Mean Age	12.58 ± 0.8	13.12 ± 0.8	12.94 ± 0.8	14.69 ± 0.9	14.93 ± 1.0

Appendix Table 5

Appendix Table 5. ^{3}He ages from Mauna Kea, Hawaii, recalculated using the Balco et al. (2008) protocol modified for ^{3}He measurements (Goehring et al., in prep). Also shown are the actual production rates used to make the calculations. Original data were calculated by Blard et al. (2007) using production rate of Blard et al. (2006), the scaling protocol of Stone (2000), and corrections for geomagnetic flux according to Dunai (2001) and Carcaillet et al. (2004). Asterisks denote weighted means for single boulder or cobble samples (MK 12C from two replicates, MK 9D and MK 11 from two phenocryst types).

Sample No.	De (ka)	Du (ka)	Li (ka)	Lm (ka)	Blard et al. (2007) published age (ka)
Production rate (atoms/g/yr)	123 ± 6	123 ± 6	131 ± 6	117 ± 6	128 ± 5
M10 moraines					
MK 12A	17.06 ± 5.5	17.68 ± 5.7	17.19 ± 5.5	18.31 ± 5.8	17.2 ± 1.7
MK 12B	18.73 ± 5	19.42 ± 5.7	18.84 ± 5.5	20.11 ± 5.9	19.1 ± 1.9
MK 12C	18.22 ± 5.5	18.9 ± 5.7	18.34 ± 5.6	19.56 ± 5.9	18.6 ± 1.9
MK 12C*	18.35 ± 5.5	19.03 ± 5.7	18.46 ± 5.6	19.7 ± 5.9	Rep
Age Range	**17.06 – 18.73**	**17.68 – 19.42**	**17.19 – 18.84**	**18.31 – 20.11**	**17.2 – 19.1**
Mean Age	18.09 ± 0.7	18.76 ± 0.8	18.21 ± 0.7	19.42 ± 0.8	18.3 ± 1.0
M2 moraines					
MK 9A	10.84 ± 3.5	11.32 ± 3.6	11.04 ± 3.6	11.91 ± 3.8	12.1 ± 1.2
MK 9B	9.32 ± 2.3	9.77 ± 2.4	9.55 ± 2.4	10.21 ± 2.6	9.8 ± 1.0
MK 9D	10.14 ± 3.5	10.6 ± 3.7	10.35 ± 3.6	11.11 ± 3.8	10.6 ± 1.1
MK 9D*	9.92 ± 3.5	10.37 ± 3.7	10.13 ± 3.7	10.86 ± 3.8	Rep
MK 9F	13.85 ± 3.5	14.41 ± 3.6	14.03 ± 3.5	15.15 ± 3.8	14.6 ± 1.5
MK 10A	14.62 ± 4.6	15.19 ± 4.8	14.78 ± 4.7	15.97 ± 5.1	15.7 ± 1.6
MK 10B	17.6 ± 4.5	18.31 ± 4.7	17.71 ± 4.6	19.29 ± 5.0	18.9 ± 1.6
MK 10C	13.97 ± 4.7	14.52 ± 4.8	14.13 ± 4.7	15.27 ± 5.1	14.9 ± 1.5
MK 11	13.01 ± 5.7	13.55 ± 5.9	13.19 ± 5.8	14.28 ± 6.3	14.5 ± 1.5
MK 11*	14.01 ± 4.6	14.56 ± 4.7	14.17 ± 4.6	15.33 ± 5.0	Rep
Age Range	**9.32 – 17.6**	**9.77 – 18.31**	**9.55 – 17.71**	**10.21 – 19.29**	**9.8 – 18.9**
Mean Age	12.73 ± 2.6	13.26 ± 2.7	12.91 ± 2.6	13.94 ± 2.9	13.9 ± 3.0